Droplet impact of Newtonian fluids and blood on simple fabrics

Effect of fabric pore size and underlying substrate

De Goede, T.C.; Moqaddam, A.M.; Limpens, K.C.M.; Kooij, S.A.; Derome, D.; Carmeliet, J.; Shahidzadeh, N.; Bonn, D.

DOI
10.1063/5.0037123

Publication date
2021

Document Version
Final published version

Published in
Physics of Fluids

License
Other

Droplet impact of Newtonian fluids and blood on simple fabrics: Effect of fabric pore size and underlying substrate

Cite as: Phys. Fluids **33**, 033308 (2021); https://doi.org/10.1063/5.0037123
Submitted: 11 November 2020 • Accepted: 25 January 2021 • Published Online: 08 March 2021

T. C. de Goede, A. M. Moqaddam, K. C. M. Limpens, et al.

Physics of Fluids ARTICLE scitation.org/journal/phf

Droplet impact of Newtonian fluids and blood on simple fabrics: Effect of fabric pore size and underlying substrate

Cite as: Phys. Fluids **33**, 033308 (2021); doi: 10.1063/5.0037123
Submitted: 11 November 2020 · Accepted: 25 January 2021 ·
Published Online: 8 March 2021

View Online Export Citation CrossMark

T. C. de Goede,[1,a)] A. M. Moqaddam,[2,3] K. C. M. Limpens,[1] S. A. Kooij,[1] D. Derome,[4] J. Carmeliet,[2] N. Shahidzadeh,[1] and D. Bonn[1,b)]

AFFILIATIONS

[1]Van der Waals-Zeeman Institute, Institute of Physics, University of Amsterdam, Science Park 904, 1098 XH Amsterdam, The Netherlands
[2]Chair of Building Physics, Department of Mechanical and Process Engineering, ETH Zurich, 8092 Zurich, Switzerland
[3]Laboratory for Multiscale Studies in Building Physics, Empa, Swiss Federal Laboratories for Materials Science and Technology, 8600 Dubendorf, Switzerland
[4]Department of Civil and Building Engineering, Université de Sherbrooke, 2500, boul. de l'Université, Sherbrooke, Québec, Canada

[a)]Electronic mail: T.CdeGoede@uva.nl
[b)]Author to whom correspondence should be addressed: d.bonn@uva.nl

ABSTRACT

When a droplet impacts a fabric mesh at a sufficiently high impact velocity, it not only spreads over the fabric but also penetrates its pores. To determine the influence of this liquid penetration of the fabric on droplet spreading on thin fabric meshes, we measured the droplet spreading ratio on fabric with and without an underlying substrate using a high-speed camera. For fabrics without a substrate, the droplet spreading ratio is reduced as the fabric penetration by the liquid reduces the droplet volume spreading on top of the fabric. Using entropic lattice Boltzmann simulations, we find that the lower droplet spreading ratio on fabrics, both with and without a substrate, is due to an increase in viscous losses inside the droplet during spreading. Comparing droplet impact of blood with its Newtonian counterpart, we show that for spreading on fabrics, just like on smooth surfaces, blood can be approximated as a Newtonian fluid.

I. INTRODUCTION

Although the impact of a droplet onto a surface is a commonly occurring phenomenon, it has proven to be an interesting field of study due to the intricate interplay between inertial, capillary, and viscous forces inside the droplet during impact. Studies have shown that a wide range of interesting physical phenomena during impact can occur: the droplet can simply spread over the surface,[1–4] but small satellite droplets can also detach from the droplet due to the interaction with the surrounding air (splashing) at high impact velocities.[5–7] Droplets can even completely bounce off the surface.[8–10] These phenomena depend not only on fluid parameters such as viscosity or surface tension, but also on the atmospheric conditions of the surrounding gas[11–16] and surface properties such as wettability[4] and surface roughness.[17]

During impact, a droplet with initial diameter D_0 hits a surface at an impact velocity v, spreading out until it reaches a maximum spreading diameter $D_{\max}$. Recent studies[1,2,18] have established the relationship between droplet spreading ratio D_{max}/D_0 and density ρ, shear viscosity η, and surface tension σ of the fluid by interpolating between two droplet spreading regimes where the kinetic energy of the droplet is either fully transformed into surface energy (capillary regime; $D_{max}/D_0 \propto \mathrm{We}^{1/2}$)[19] or fully dissipated by the viscous forces inside the droplet (viscous regime; $D_{max}/D_0 \propto \mathrm{Re}^{1/5}$).[20,21] Here, We and Re are the Weber ($\mathrm{We} \equiv \rho D_0 v^2/\sigma$) and Reynolds ($\mathrm{Re} \equiv \rho D_0 v/\eta$) numbers, respectively. For low impact velocities, the wettability of the surface can also be incorporated into the droplet spreading model by using the spherical cap model.[2,4,22] Other spreading models have also been proposed, either by considering the viscous dissipation in the shear boundary layer for inelastic impacts on no-slip surfaces,[3] or by analytically calculating the fluxes and momentum during droplet spreading.[23]

While droplets spreading on smooth surfaces has received ample attention, droplet spreading on fabrics has not yet been studied extensively, despite its relevance to fields such as crime scene investigation

and the textile industry. The fabric substrate complicates the physical picture. For example, absorption of liquid by the yarns of the fabric due to capillary action (wicking)[24–26] could heavily influence the long timescale dynamics of droplet spreading. But even if the droplet is not absorbed by the fabric yarns, droplet spreading is still significantly different compared to droplet spreading on smooth surfaces. For example, recent studies on monofilament (fabric) meshes have shown that droplets penetrate through the pores of the mesh if their impact velocity is high enough, allowing a part of the droplets to pass through the mesh.[27–32] Several studies also showed that, at high Weber numbers, from the moment the fabric or mesh is penetrated, the droplet spreading ratio on fabrics is significantly lower than expected from the scaling models used in these studies.[30,31] Understanding how droplet spreading is influenced by the roughness of the fabric, liquid penetration of the (fabric) mesh and whether the preexisting spreading model of Refs. 1 and 2 could be used to predict droplet spreading on these fabrics could have significant practical applications in, for example, the textile industry[33,34] and forensic research.[35–38] For forensic applications, the liquid of most interest is blood. As a result, it is also important to determine whether the shear thinning properties of blood have an influence on droplet spreading. For droplet impact on smooth surfaces, Laan *et al.*[1] have shown that the high shear rate exerted on a droplet during spreading allows blood to be approximated as a Newtonian fluid during droplet impact, with a viscosity given by the high-shear-rate viscosity η_∞. In this specific case, the question is whether the same approximation holds for droplets spreading over fabric meshes, or if the liquid penetration of the fabric might lead to some shear thinning effects that do not occur on a smooth surface. A final question inspired by real-world experimental scenarios is how a solid substrate located underneath a fabric would influence the droplet spreading process, and whether the patterned roughness of the fabric, given by the geometry of the pores and fibers of the fabric, has an influence on droplet spreading on fabrics.

In this study, we investigate the influence of fabric roughness and liquid penetration of fabrics on droplet spreading for plain woven monofilament polyester meshes. Using high-speed imaging, we show that the liquid penetration decrease in droplet spreading can be ascribed to part of the volume of the droplet passing through the fabric, in agreement with earlier studies. We find that, even if the downward flow of liquid beyond the fabric mesh is blocked by an underlying substrate, at high impact velocities ($v > 1$ m/s), the droplet spreading ratio is still lower than that of smooth surfaces. This difference is due to an increased viscous dissipation inside the droplet during spreading caused by the well-defined patterned roughness of the fabric, as we conclude from combining experimental results and entropic lattice Boltzmann simulations. These simulations indicate that this increase in viscous dissipation is due to the liquid flow into the pores of the fabric and to the droplet pushing itself between the fabric and substrate at velocities above the penetration velocity. We find that the shear thinning properties influence fabric penetration but not droplet spreading on top of the fabric, allowing blood to be approximated as a Newtonian fluid when considering droplet spreading on top of thin fabric meshes.

II. METHODS

A. Experiments

To measure the spreading ratio of an impacting drop, a 0.4 mm-diameter blunt-tipped needle (BBraun Sterican) was used to generate droplets with an initial diameter D_0 of 2.29 ± 0.06 mm falling from a variable height onto a substrate, making the droplet release method reproducible within a relative error of 2.5%. The generated droplets were spherical during free fall, indicating that the droplets were sufficiently smaller than the capillary length of a water drop (2.7 mm) for gravity effects to be neglected in this study. By systematically changing the height of the needle, the maximum spreading diameter D_{max} was investigated as a function of the impact velocity v_{imp} using high-speed imaging with a frame rate between 4004 and 8100 fps and spatial resolutions between 11 and 17.7 μm per pixel. Droplet impact measurements were performed on a stainless steel surface as reference (average roughness $R_a = 0.247 \pm 0.007 \mu$m as measured by a Keyence VK-X1000 laser scanning confocal microscope). As fabrics, single cylindrical polyester fibers were woven in a crisscross pattern, creating a polyester mesh with rectangular pores [Fig. 1(a); Gilson Company Inc.]. These single fiber yarn fabrics were chosen to eliminate any influence of liquid imbibition by the fabric on droplet spreading. Three different monofilament polyester fabrics were used, each with a different pore size and yarn thickness (see Table I). Each pore size for the fabrics was chosen such that the pore size was much smaller than the initial diameter D_0. For the polyester fabrics, droplet impact was measured on fabrics that were either spanned over a small gap of roughly 8 mm (a fabric without a substrate) or placed on a steel substrate

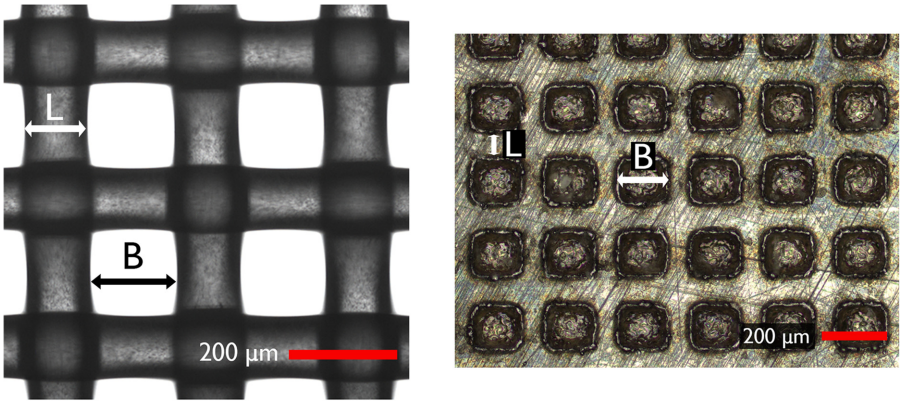

(a) (b)

FIG. 1. (a) A microscope image of a plain woven monofilament polyester fabric. (b) An image of a patterned surface made with an optical laser microscope (Keyence VK-X1000). The average measured depth of the holes is equal to 64 ± 1 μm. Pore size *B* and pore spacing (or yarn diameter) *L* are denoted in both figures.

TABLE I. Pore size and spacing of the fabrics and patterned surface used.

System	Pore size B (μm)	Pore spacing L (μm)
Fabric	45	40
Fabric	106	70
Fabric	150	80
Patterned surface	135	76

(fabric with substrate). The fabric was spanned tight both over the gap and on the substrate using magnetic clamps to minimize unwanted energy loss due to fabric movement[30,39,40] or any influence of the tension exerted on the fabric.[32] In this study, it was assumed that the polyester fibers were rigid and do not deform during droplet impact. Placing the fabric on a substrate blocks the downward liquid flow when the fabric is penetrated, allowing us to investigate the effect of droplet penetration on droplet spreading. Droplet impact was also compared between plasma-treated fabrics and untreated fabrics to investigate the influence of fabric wettability on droplet spreading. Fabrics were plasma treated for 6 min on both sides to guarantee that the wettability was increased evenly across the whole fabric.

Droplet spreading was also measured on a patterned surface: a steel surface in which rectangular holes were cut using an electrical discharge machining method[41] [Fig. 1(b)]. The size, depth, and spacing of the holes were chosen in such a way that the dimensions of the pores of the patterned surface were similar to that of the 150-μm fabric (see Table I). Droplet impact measurements on the patterned surface were compared to the droplet impact measurements on the smooth surface and fabrics. This allowed us to investigate the influence of the roughness of the fabrics/patterned surfaces as a result of the presence of the pores.

For most experiments, demineralized water was used (density $\rho = 998\,\mathrm{kg/m^3}$, surface tension $\sigma = 72\,\mathrm{mN/m}$, and viscosity $\eta = 1\,\mathrm{mPa\,s}$). Droplet impact of a 1:1 water–glycerol mixture ($\rho = 1124\,\mathrm{kg/m^3}$, $\sigma = 65.75\,\mathrm{mN/m}$, and $\eta = 4\,\mathrm{mPa\,s}$) was measured on both a smooth surface and 150-μm fabric. The water–glycerol measurements on a smooth surface were compared to droplet spreading of water on fabric, while the water–glycerol mixture measurements on the 150-μm fabric were compared to blood spreading on fabric. These two measurements were compared to investigate the influence of the shear thinning properties of blood on droplet spreading. The properties of blood ($\rho = 1055\,\mathrm{kg/m^3}$, $\sigma = 59\,\mathrm{mN/m}$, and high shear rate viscosity $\eta_\infty = 4.8\,\mathrm{mPa\,s}$) were obtained from Ref. 1. They determined η_∞ using the Sisko model [$\eta(\dot\gamma) = \eta_\infty + k\dot\gamma^{n-1}$ (Ref. 42)], where $\dot\gamma$ is the shear rate and k and n are fitting parameters, which were equal to 38 mPa s^n and 0.41 in the study of Laan *et al.*, respectively. Sodium citrate was added to blood to prevent coagulation during the experiments. The surface tension of blood was found to increase with roughly 3 mN/m for a sodium citrate concentration of 10%. Since the amount of sodium citrate that was added to the blood in this study was small (~2.5% mass concentration), we assume the change in surface tension due to the anticoagulant to be negligible. Red blood cells are heavy enough to sediment due to gravity. To prevent any sedimentation to form inside the droplet, the needle was cleaned by generating several droplets before the measurement to ensure a consistent concentration of red blood cells inside the blood droplet during spreading.

B. Simulations

For 3D numerical simulations, the recently tested and validated entropic lattice Boltzmann method for two-phase flows was used.[43] Here, a brief overview of the simulations will be discussed together with a short clarification on the numerical setup and simulated parameters used in this study. The goal is to provide a general overview of the used simulations. More detailed information and validation of these simulations with experimental studies is discussed in detail elsewhere.[44–49]

The software is an integrated in-house code written in Fortran 90, which is capable of simulating incompressible flows, multiphase flows, and porous media flows with complex geometry. It is fully parallelized using a Message Passing Interface (MPI) for communication, allowing for the simulation to be computed using multiple cores. The simulations are conducted with the HPC of Swiss National Supercomputing Center, specifically with the XC40 nodes [Two Intel® Xeon® E5–2695 v4 at 2.10 GHz (2 × 18 cores, 64/128 GB RAM)] of the supercomputer Piz Daint. The simulated domain is 700 × 700 × 400 grid nodes [Fig. 2(a)] and the typical droplet impact simulation had a total time frame between 7.5 and 9.6 ms. The computation time of the simulations, using 2304 CPU's, was between 178 and 274 min.

For a liquid–vapor system separated by an interface, the entropic lattice Boltzmann equation reads as

$$f_i(\boldsymbol{x} + \boldsymbol{v}_i\delta t, t + \delta t) = f_i(\boldsymbol{x}, t) + \alpha\beta\left[f_i^{\mathrm{eq}}(\rho, \boldsymbol{u}) - f_i(\boldsymbol{x}, t)\right] + \left[f_i^{\mathrm{eq}}(\rho, \boldsymbol{u} + \delta\boldsymbol{u}) - f_i^{\mathrm{eq}}(\rho, \boldsymbol{u})\right], \quad (1)$$

where $f_i(\boldsymbol{x}, t)$ are the discrete populations and v_i $(i = 1, \ldots, N)$ denote the discrete velocities corresponding to the underlying lattice structure. The D3Q27 lattice ($N = 27$) was used for our three-dimensional simulations. Parameter β $(0 < \beta < 1)$ was determined using the kinematic viscosity, $\nu = c_s^2\delta t[1/(2\beta) - 1/2]$, with $c_s = \delta x/\left(\sqrt{3}\delta t\right)$ the lattice speed of sound and $\delta x = \delta t = 1$ as lattice units. The equilibrium population f_i^{eq} was used as the minimizer of the discrete entropy function,

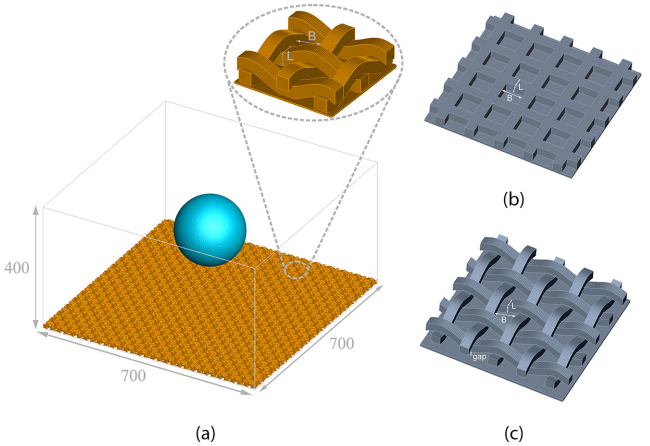

FIG. 2. (a) A 3D simulation setup showing a droplet above a fabric-like geometry before impact. Droplet impact was simulated in three dimensions for geometries representing a smooth surface (not shown), a patterned surface (b), and a fabric (c). The pore size and yarn diameter for the latter two cases correspond to the 150-μm fabric investigated experimentally (Table I). The fabric (c) was either attached to a substrate or placed above a substrate with a small gap of around 35 μm.

$H = \sum_{i=1}^{N} f_i \ln(f_i/W_i)$, under the constraints of local mass and momentum conservations, $\{\rho, \rho\boldsymbol{u}\} = \sum_{i=1}^{N}\{1, \boldsymbol{v}_i\}\{f_i^{eq}\}$, where W_i are the lattice weights. The stabilizer parameter α defines the maximal overrelaxation, which is computed from the entropy estimate equation at each time step for each computational node.[45]

In Eq. (1), the two-phase effects resulting from intermolecular forces are present through the velocity increment $\delta\boldsymbol{u} = (\boldsymbol{F}/\rho)\delta t$, with the force $\boldsymbol{F}$ being the sum of the fluid–fluid ($\boldsymbol{F}_{f-f}$) and fluid–solid interactions ($\boldsymbol{F}_{f-s}$). Phase separation occurs by defining the fluid–fluid interaction as $\boldsymbol{F}_{f-f} = \nabla\cdot(\rho c_s^2\boldsymbol{I} - \boldsymbol{P})$ using the Korteweg's stress $\boldsymbol{P}$ as

$$\boldsymbol{P} = \left(p - \kappa\rho\nabla^2\rho - \frac{\kappa}{2}|\nabla\rho|^2\right)\boldsymbol{I} + \kappa(\nabla\rho)\otimes(\nabla\rho), \tag{2}$$

where κ is the coefficient controlling the surface tension, $\boldsymbol{I}$ is the unit tensor, and p denotes the nonideal equation of state,[50] for which the Peng–Robinson equation was used.[51] The introduction of a cohesive interaction through the velocity increment in Eq. (1) leads to the surface tension forces separating the liquid and vapor by an interface, which maintains the liquid and vapor in an equilibrium state. The wettability condition is modeled by taking into account the fluid–solid interaction $\boldsymbol{F}_{f-s}$,

$$\boldsymbol{F}_{f-s}(\boldsymbol{x}, t) = \kappa_w\rho(\boldsymbol{x}, t)\sum_{i=1}^{N} w_i s(\boldsymbol{x} + \boldsymbol{v}_i\delta t)\boldsymbol{v}_i, \tag{3}$$

where the strength of the fluid–solid interaction is reflected by κ_w. The indicator function $s(\boldsymbol{x} + \boldsymbol{v}_i\delta t)$ in Eq. (3) is equal to one for solid nodes, but zero otherwise. w_i are the weight coefficients.[44]

In the simulation, the droplet ($D_0 = 2.3$ mm) was initially placed at a certain height above the fabric. As gravity effects could be neglected in the experiments, these were also not considered in the simulations. Both liquid and vapor phases were first initialized by imposing a zero impact velocity, after which the simulations were run for a short period of time to allow the liquid–vapor interface to reach equilibrium. Then, a uniform impact velocity V_i toward the surface was imposed on the liquid droplet. The liquid density, vapor density, and interfacial surface tension of the simulated droplet were determined using the ratio of $\rho/\rho_c = 3.06$ (liquid to critical density ratio), $\rho_v/\rho_c = 0.028$ (vapor to critical density ratio), and $\sigma/p_cD_0 = 0.0296$ [corresponding to $\kappa = 0.00468$ in Eq. (2)], respectively. The critical density ρ_c was computed at the critical temperature T_c and critical pressure p_c from the Peng–Robinson equation of state.[51] The temperature ratio ($\frac{T}{T_c}$) used in this study is equal to 0.73, far from the critical point. The critical density was calculated to accurately model the evolution of the liquid–vapor phase during droplet impact. Previous studies have shown that the spurious current gets higher with density ratio, which affects both the stability and accuracy of the simulations. However, these studies have also shown that the liquid to vapor density ratio of around 110 is more than sufficient to correctly capture the dynamics of droplets impacting on solid substrates;[48,52] which was used in this study. The dynamic viscosity η of the liquid is set according to the Ohnesorge number $[Oh = \eta/\sqrt{(\rho\sigma D_0)}]$ for the simulated water droplet. The pore size B and spacing L [Fig. 2(a)] are determined by keeping the aspect ratio of the droplet diameter to the pore size and pore spacing the same as in the experiments. The equilibrium solid–liquid static contact angle in the simulations is set to 70°, comparable to the contact angle of polyester.[53] With the current method of imposing the contact angle on the simulations, it is not possible to consider contact angle hysteresis on smooth surfaces. However, it would be possible to do this for micro-structured surfaces, as was shown in a previous study.[49] However, if we only impose the equilibrium contact angle in the simulations, we show in Sec. III D that the simulation results for the fabrics agree very well with their experimental counterpart. Therefore, in this study, the contact angle hysteresis does not seem to have a significant influence during droplet spreading on monofilament fabrics.

The size of the computational domain was determined using a grid independence study, giving a domain of $700 \times 700 \times 400$ grid nodes. Periodic boundary conditions were applied at the edges, where a wall boundary condition similar to Ref. 44 was used for the top and bottom edges of the simulation domain as well as the solid surfaces.

Droplet impact was simulated for multiple surfaces similar to the surfaces used in the experiments. A smooth surface was used as a reference. The simulated patterned surface [Fig. 2(b)] had holes of the same dimensions as the pores of the 150-μm fabric. The fabric was recreated in the simulations by weaving rectangular "fibers" in a sinusoidal pattern, similar to the plain weave of the fabric used in the experiments. Droplet impact was simulated for both a fabric placed on a substrate and a fabric suspended in the air. For the former, droplet impact was simulated for cases where the fabric was attached to the substrate (no flow between the fabric and substrate), or placed above the substrate with a small gap of around 35 μm between the fabric and substrate, allowing for a flow of liquid between the two. For all simulations, the simulated fibers were considered to be rigid during droplet impact.

III. RESULTS AND DISCUSSION

A. Droplet impact and fabric penetration

Figure 3(a) shows high-speed images of a water droplet at maximum spreading on stainless steel (top row), fabrics with substrate (middle row), and a fabric without a substrate (bottom row). Similar to earlier studies,[30,31] the droplet penetrates through the fabric without a substrate when the impact velocity is high enough. Consequently, the measured droplet spreading ratio [Fig. 3(b)] of fabrics with and without a substrate starts to deviate at the moment the droplet penetrates the fabric. The threshold impact velocity at which the droplet penetrates the fabric, the penetration velocity, is dependent on the pore size. By increasing the impact velocity of the droplet until the droplet starts to penetrate the fabric, the penetration velocity of the 45 μm and 150 μm fabric was experimentally determined to be 1.5 ± 0.1 m/s and 0.8 ± 0.1 m/s, respectively. The data are shown in the form of D_{max}/D_0 as a function of the impact velocity instead of the Weber number as the droplet spreading ratio is not only dependent on the Weber number, but the Reynolds number and surface wettability as well.[1,2,4,18] Finally, it is important to note that the results and discussion given below apply to fabrics with pores size that are much smaller than the initial diameter of the impacting droplet (D_0 is roughly 51 to 15 times larger than the pore size B for the 45 and 150 μm fabrics, respectively).

A droplet can only penetrate a hydrophobic fabric (or mesh) when the dynamic pressure of the droplet exerts on the fabric ($\sim\rho v^2$) which is high enough to overcome the resisting capillary pressure ($\sim 4\sigma/B$) of the pores. Ryu *et al.* showed that it is possible to calculate

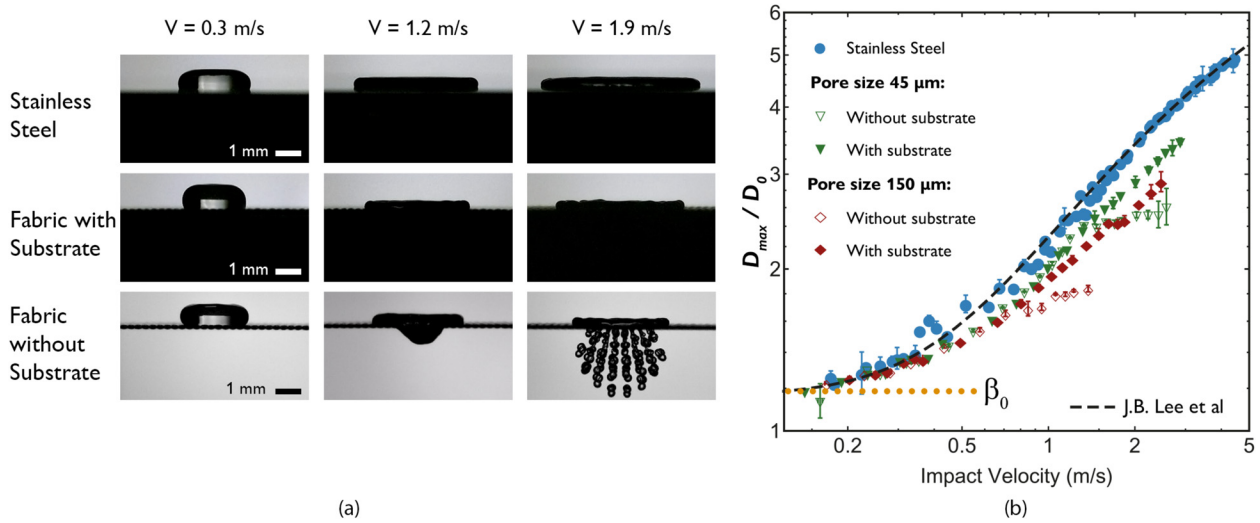

FIG. 3. (a) High-speed images of droplets at maximum spreading on stainless steel (top), a fabric with a substrate (middle), and a fabric without a substrate (bottom) at different impact velocities, increasing from left to right. The pore size of the fabric depicted here is 150 μm. (b) Measured spreading ratio as a function of the impact velocity for fabrics with pore sizes of 150 μm (red symbols) and 45 μm (green symbols) compared to the droplet spreading ratio on stainless steel (blue circles), and the theoretical prediction of Lee *et al.* [Eq. (9)] for droplet spreading on smooth surfaces (black dashed line). At low impact velocities, the spreading ratio reaches a constant value at zero velocity (β_0; orange dotted line). The filled and open symbols indicate whether the fabric was placed on a substrate or suspended in the air, respectively.

the penetration velocity v_p at which a mesh is penetrated by balancing these pressures,[28]

$$v_p = \sqrt{\frac{4\sigma}{C_0 \rho B}}, \tag{4}$$

where C_0 is a proportionality constant, which is equal to 2.78 for plain woven meshes with rectangular pores.[28] The above equation can also be found when a critical Weber number We^* is introduced for which the droplet penetrates the fabric, given by

$$We^* \equiv \frac{\rho B v_p^2}{\sigma}. \tag{5}$$

Rewriting the above equation results in a similar equation as Eq. (4), where $4/C_0 = We^*$. Calculating the critical Weber number for the 45 and 150 μm fabrics yields 1.40 and 1.33, respectively, and agrees well with the constant given by Ryu *et al.* ($4/C_0 = 1.44$). Using Eq. (4), we find penetration velocities of around 1.52 m/s and 0.83 m/s for the 45 μm and 150 μm fabrics, respectively, agreeing very well with the penetration velocity determined from the drop impact measurements. Thus, the liquid penetration of the fabric indeed has a significant influence on droplet spreading, in agreement with previous studies.

Fabric penetration by the droplet is also dependent on the wettability of the fabric.[54–56] The effect of fabric wettability on the liquid penetration of the fabric can be observed when a droplet is gently placed on the untreated fabric [Fig. 4(a)] or plasma treated fabric [Fig. 4(b)]. For the untreated fabric, the droplet remains on top of the fabric, resulting in a high contact angle on the fabric (116° ± 3°).

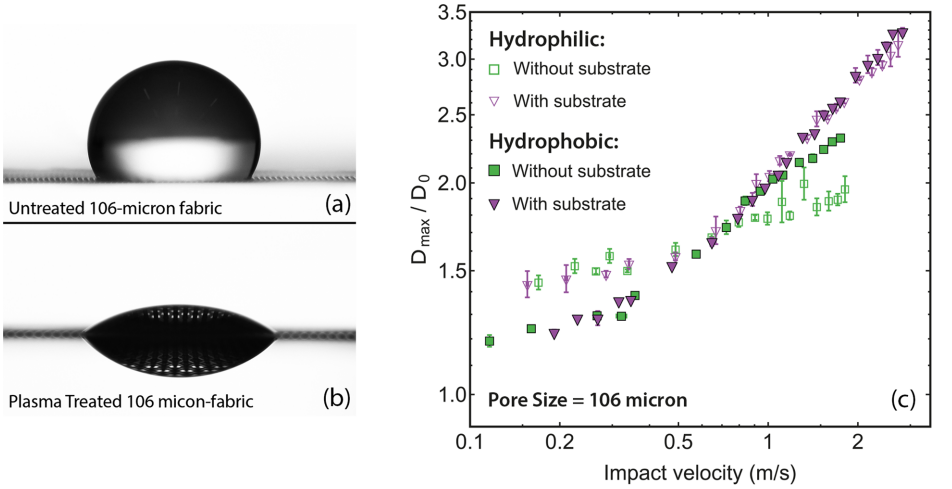

FIG. 4. Gently deposited water droplet at mechanical equilibrium on untreated (low wettability) (a) and plasma treated (high wettability) and (b) 106-μm fabrics suspended in the air. (c) Measured spreading ratio on plasma-treated (hydrophilic; open symbols) and untreated (hydrophobic; filled symbols) 106-μm fabrics. Fabrics were placed on a substrate (purple triangles) or spanned over a small gap of air (green squares). The dashed black line is the theoretical prediction by Lee *et al.* [Eq. (9)] for droplet spreading on a smooth surface.

When the wettability of the fibers is increased with the plasma treatment, the droplet penetrates the pores and wet both sides of the fabric. The resulting contact angle of the top part of the droplet is significantly lower ($38^\circ \pm 3^\circ$) compared to the untreated fabric. The contact angle on both the untreated and plasma treated fabrics was measured directly from images similar to Figs. 4(a) and 4(b) using *ImageJ*. These contact angles were measured thrice and averaged, where the uncertainty is given by the standard deviation. Do note that these fabric contact angles are not equal to the contact angle of the polyester fibers, which could not be measured in this study. However, these images do show that the plasma treatment significantly changes the wettability of the fabric and has an influence on how the droplet interacts with the fabric during spreading.

The change in wettability by the plasma treatment also influences droplet spreading on top of the fabric. First, increasing the wettability of the fabric increases the droplet spreading ratio at low impact velocities, both for the fabrics with and without substrates [Fig. 4(c)]. This is a similar effect to that is observed when the wettability is increased for smooth surfaces.[4] The second wettability effect on droplet spreading is that it reduces the droplet spreading ratio on plasma-treated fabrics without substrate (open green squares in Fig. 4) compared to the droplet spreading ratio on untreated fabrics without substrate (filled green squares). Comparing high-speed videos of the untreated fabric and plasma treated fabric (Movies 1 and 2 in the supplementary material, respectively) reveals that the increased wettability results in more liquid being pushed through the fabric, as the higher wettability results in a lower capillary pressure inside the pores. The larger amount of liquid passing through the fabric subsequently reduces the droplet spreading ratio as less volume is left on top of the fabric to spread outwards.

A reduction in droplet volume on top of the fabric influences the spreading difference between fabrics with and without substrate underneath. Due to the volume reduction, the initial diameter D_0 overestimates the actual liquid volume spreading on top of the fabric, decreasing the droplet spreading ratio. To correct for this volume loss, we experimentally estimate the liquid volume that penetrates the (untreated) fabric. At the moment the maximum amount of liquid has passed through the fabric [Fig. 5(a)], the maximum volume of the penetrated liquid V_{pen} can be estimated from the image by assuming the liquid underneath the fabric takes the shape of a paraboloid [Fig. 5(a)] and its volume can be determined by measuring its base radius a and height h,

$$V_{pen} = \frac{\pi}{2} a^2 h. \tag{6}$$

By subtracting V_{pen} from the volume of the droplet, an adjusted initial diameter D_0^* can be determined, and with it the volume-corrected spreading ratio,

$$\frac{D_{max}}{D_0^*} = \frac{D_{max}}{\sqrt[3]{D_0^3 - 3a^2 h}}. \tag{7}$$

Using the above equation, the volume loss corrected spreading ratio [gray symbols; Figs. 5(b) and 5(c)] on both the 150 μm [Fig. 5(b)] and 45 μm [Fig. 5(c)] fabrics without a substrate is determined for every drop impact measurement above the penetration velocity. The volume correction for both fabrics works very well, as the spreading ratios of the fabric with and without substrate become comparable after the volume correction is applied. For the 45-μm fabric, we still observe a slightly lower spreading ratio for fabrics without substrate after the volume correction. This is likely due to the liquid below the fabric attaining an irregular shape when it coalesces underneath the fabric, making the volume estimation with a paraboloid less accurate for the 45-μm fabric. Nevertheless, these results show that the difference in spreading for the fabric with and without a substrate is fully determined by the loss of liquid when the droplet penetrates the fabric.

If the droplet impacts a fabric without a substrate fast enough, the penetrating liquid moves too fast to coalesce underneath the fabric

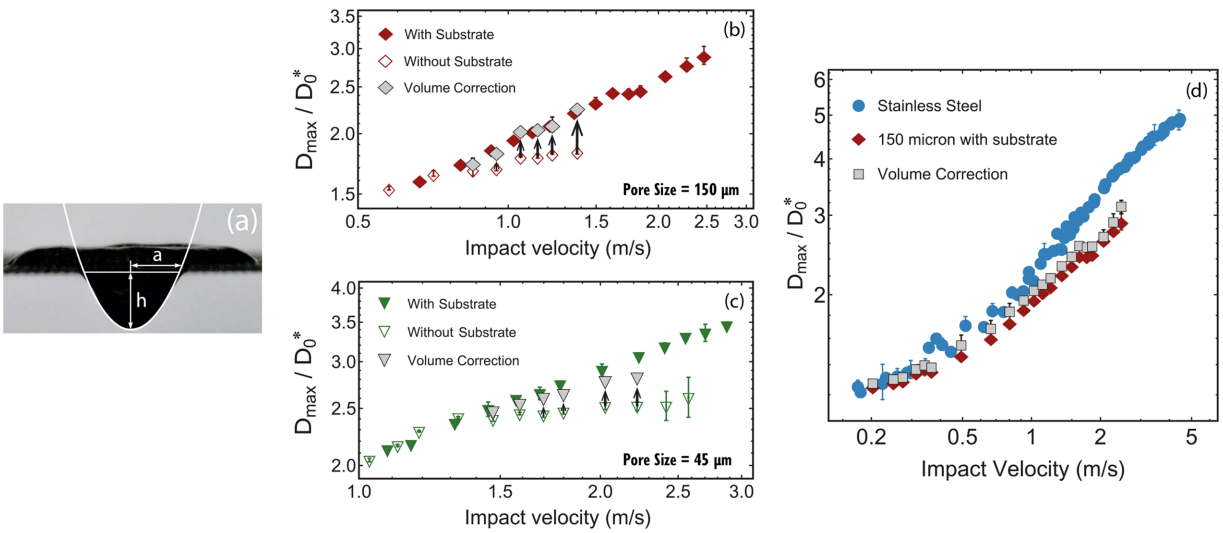

FIG. 5. (a) Photograph of an impacting drop on the fabric without a substrate at the moment the amount of liquid below the fabric is largest, with the white line a paraboloid of base radius *a* and height *h*. [(b) and (c)] Spreading ratios as a function of impact velocity for 150 μm (b) and 45 μm (c) pore-size fabrics with and without a substrate, with the latter values also corrected for liquid loss due to fabric penetration using Eq. (7) (grey symbols). (d) Spreading ratios for a smooth reference surface (blue symbols) and a 150-μm fabric with a substrate, both without (red diamonds) and with (grey squares) correction for the volume lost inside the pores [Eq. (8)].

and liquid remain separated as liquid "fingers" instead. These fingers subsequently break up into many droplets, resulting in a spray where the droplets that are on the order of 100 μm in size [Fig. 3(a); bottom right]. Droplet fragmentation below a mesh in itself is a fascinating phenomenon, attracting interest due to several recent studies as it could be used as a novel method to create sprays,[27,29] although it was recently shown that it currently performs poorly compared to other atomization methods.[32] As the main focus of this study lies on droplet spreading on top of the fabrics, however, droplet fragmentation is not discussed here.

Being able to correct for the volume loss during droplet spreading on fabrics without a substrate, we can now compare droplet spreading on fabrics with droplets spreading on smooth surfaces [Fig. 3(b)]. At low impact velocities ($v < 1$ m/s), no significant difference can be observed between droplets spreading on fabrics with a substrate and smooth surfaces. For high velocity droplet impacts ($v > 1$ m/s), however, the droplet spreading ratio on the fabrics with substrates is significantly lower compared to the droplet spreading ratio on the smooth surface. This deviation increases with increasing pore size.

We next investigate whether this difference in spreading is also due to a loss of liquid volume, as part of the droplet is used to fill up the pores of the fabric. With the assumptions that the pores are rectangular (with volume of B^2L) and that all pores underneath the droplet at maximum spreading are filled, it is possible to estimate the total droplet volume loss on the fabric with a substrate at maximum spreading, assuming there is no gap between the fabric and substrate,

$$V_{pen} = N_p V_p = \frac{\pi}{4} D_{max} \frac{B^2 L}{(B+L)^2}, \tag{8}$$

where N_p is the number of filled pores and V_p is the volume of a single pore. Correcting the volume loss using Eqs. (7) and (8) shows that the lost volume is too small to account for the difference in spreading between a fabric with a substrate and smooth surfaces [Fig. 5(d)]. Thus, the difference in the droplet spreading ratio between the smooth surfaces and fabrics has to be due to a different mechanism entirely, which is obviously due to the roughness of the fabric.

B. Viscous dissipation

To qualitatively understand the difference in droplet spreading for the fabrics and smooth surface, a model describing the mechanisms of droplet spreading is needed. In recent years, several droplet spreading models have been proposed such as the spreading models of Laan *et al.*,[1] Lee *et al.*,[2] Wildeman *et al.*,[3] and Gordillo *et al.*[23] Each of these spreading models have their advantages and disadvantages. For example, the spreading models of Wildeman *et al.* and Gordillo *et al.* can be applied to a wider range of droplet impact phenomena, such as incorporating the influence of the Leidenfrost effect on droplet spreading. The spreading models of Laan *et al.* and Lee *et al.* in contrast are easier to use, as the droplet spreading ratio does not have to be integrated[23] or solved numerically[3] in the high impact velocity regime ($v > 1$ m/s). The model of Lee *et al.* does requires an extra fitting parameter however to incorporate the influence of the liquid surface tension and surface wettability. Determining which model predicts droplet spreading the best for our experiments is not the goal of this study. Therefore, we chose for the droplet spreading model of Lee *et al.* for its ease of use while giving a good prediction of the droplet spreading ratio in the impact velocity regime presented in this study.

As mentioned earlier, the kinetic energy of an impacting droplet during spreading is either transformed into surface energy or dissipated by the viscous forces inside the droplet. Eggers *et al.*, Laan *et al.*, and Lee *et al.* found a relation between the droplet spreading ratio and the impact velocity and fluid properties by interpolating between the capillary regime ($\propto \mathrm{We}^{1/2}$) and viscous regime ($\propto \mathrm{Re}^{1/5}$) using a first-order Padé approximant,[1,18] which was modified by Ref. 2 to account for low impact velocity droplet spreading,

$$\left(\frac{D_{max}}{D_0}\right)^2 - \beta_0^2 = \frac{\mathrm{We}^{1/2}}{7.6 + \mathrm{We}^{1/2}} \mathrm{Re}^{1/5}. \tag{9}$$

Here, β_0 is defined as the value of the maximum spreading ratio at zero impact velocity, which is dependent on the liquid surface tension and surface wettability.[2,4] The numerical constant 7.6 is a fitting constant obtained by means of a least squares method.[2] The above equation shows very good agreement with our experimental data for water droplets impacting the smooth surface [black line in Fig. 3(b), where β_0 was used as a fitting parameter]. Lee *et al.* also showed that the droplet spreading ratio at high impact velocities decreases when the viscosity of the liquid is increased, as viscous losses become more important at higher impact velocities. We investigate the role of liquid viscosity by comparing the droplet spreading ratio of a water–glycerol mixture impacting a smooth surface [$\eta = 4$ mPa s; orange squares in Fig. 6(a)] to that of a water droplet impacting a 150-μm fabric [Fig. 6(a)]. Interestingly, the spreading curves are similar. The comparison between the measurements suggests that changing the smooth surface to a fabric would have an equivalent effect on droplet spreading as increasing the viscosity of the fluid does. The best fit of Eq. (9) for the water–glycerol mixture also predicts the measured spreading ratio on fabrics well, allowing us to determine the spreading dynamics of water on a fabric substrate by using an "effective" viscosity higher than the viscosity of the liquid. We hypothesize that the smaller droplet spreading ratio on fabrics is due to an increase in viscous losses inside the droplet when it spreads over the fabric.

At high impact velocities ($v > 1$ m/s), the spreading dynamics of a droplet between the moment of impact and maximum spreading is dominated by the fluid's inertia: when the droplet spreading diameter $D(t)$ is rescaled with the maximum spreading diameter [Fig. 6(b)], the droplet spreading curves of water and the water–glycerol mixture collapse onto a single curve, reaching maximum spreading after 2.8 ± 0.2 ms, which is comparable to the inertial timescale, $[\tau = \sqrt{\rho(\frac{1}{2}D_0)^3/2\sigma} \approx 3.2 \pm 0.3$ ms], given by Richard *et al.* This shows that the droplet spreading dynamics of the two fluids are identical and thus independent of the liquid viscosity. Interestingly, water droplets spreading on the more complex geometry surfaces also follows the same spreading dynamics [Fig. 6(b)] as water droplets spreading on a smooth surface. Thus, the identical droplet spreading curves observed in Fig. 6(b) show that changing either the viscosity or the surface geometry only influences how far the droplet spreads, i.e., changing the maximum spreading diameter D_{max}, and not the spreading dynamics of the droplet at high impact velocities.

A likely candidate for the increased viscous dissipation inside a droplet is the roughness of the fabric, characterized by the fabric pores: when a droplet spreads over a surface, liquid enters the pores underneath the droplet until they are full, where the liquid in the pore comes

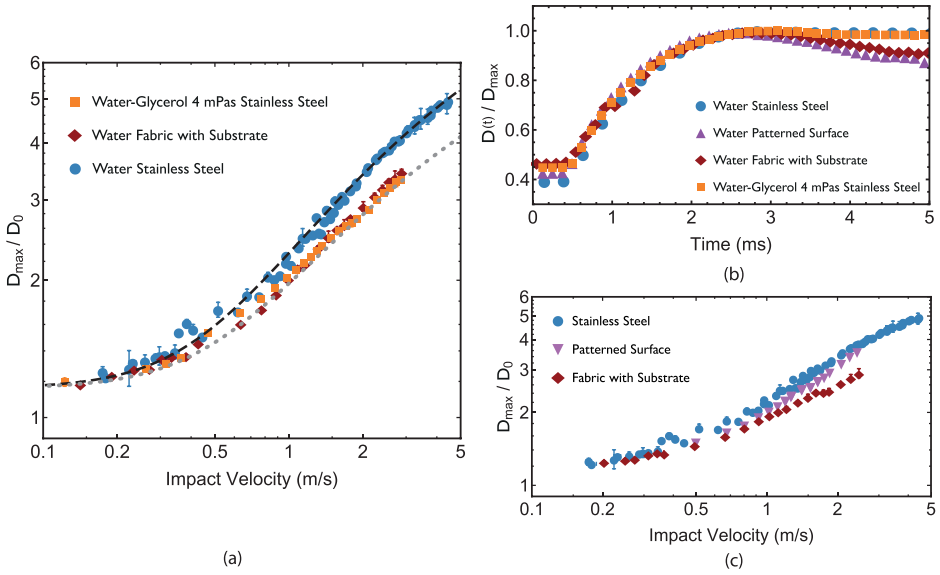

FIG. 6. (a) Measured spreading ratio for water impacting a stainless steel surface (blue circles) and a 150 μm pore size fabric with a substrate (red diamonds) compared to the measured spreading ratio of a 1:1 water–glycerol mixture (four times the viscosity of water) impacting stainless steel. The dashed and dotted lines are the best fits of the theoretical predictions of Lee *et al.* for water and water glycerol mixture impacting stainless steel, respectively. (b) Measured droplet diameter at $v \approx 1.25$ m/s as a function of time from the moment of impact ($t = 0$) for the surfaces shown in (a) and (c), rescaled with D_{max}. (c) Measured droplet spreading ratio on stainless steel (blue circles), patterned surface (purple triangles), and 150 μm fabric with a substrate.

to a full stop and the kinetic energy is dissipated by the viscous forces. The difference in droplet spreading is thus dependent on the roughness of the fabric, which is given by the pore size and yarn diameters. If that were to be true, droplet spreading on fabrics with substrate should be similar to droplet spreading on a patterned surface if the pore size and yarn thickness are comparable. We find that this is not the case [Fig. 6(c)]. Although droplet spreading on the patterned surface and 150 μm fabric are similar at first, the droplet spreading ratio of the patterned surface diverges from that of the fabric at high impact velocities. Interestingly, the droplet spreading ratios of both the fabric with a substrate and a patterned surface start to deviate at the moment the impact velocity is higher than the penetration velocity of the 150 μm fabric (0.8 ± 0.1 m/s). We thus propose that the substrate underneath the fabric blocks the downward flow of the fluid and redirects the fluid in between the fabric and substrate due to the pores of the fabric being connected. So not only does the droplet lose energy due to the pores of the fabric, the viscous losses that could be caused by the droplet pushing itself between the fabric and substrate also have to be taken into account.

C. Blood droplet impact

Before discussing the viscous losses inside droplets impacting a fabric mesh, droplet spreading of blood is discussed first. If the shear thinning properties of blood are indeed important for droplet spreading on fabrics, these properties should be taken into account for the viscous losses inside a droplet. Comparing the spreading ratio of blood (Fig. 7, red triangles) and the water–glycerol mixture (orange squares), which has a viscosity similar to the high shear rate viscosity η_∞ of blood, reveals two interesting features. First, the spreading ratios on fabric as a function of impact velocity of blood and the water–glycerol mixture (red triangles and orange squares, respectively) are roughly similar. This observation is in line with that of Ref. 1 for the same liquids spreading on a smooth surface. Second, the penetration velocity, which is the impact velocity at which the spreading curves with and without a surface underneath the fabric start deviating from each other, is different for the two liquids. For the water–glycerol mixture, it is around 1 m/s (higher than the penetration velocity of water) and for blood 1.5 m/s.

This suggests that blood penetrates the fabric less than its Newtonian counterpart. When a liquid pushes through a constriction, not only are the shear stresses important but also the elongational stresses applied on the liquids. While blood shows a non-Newtonian viscous behavior when it is sheared (e.g., a spreading droplet), studies have shown that it also exhibits a viscoelastic behavior when subjected to elongational stresses.[57–59] This viscoelastic behavior in the extensional flow could cause more resistance against fabric penetration,

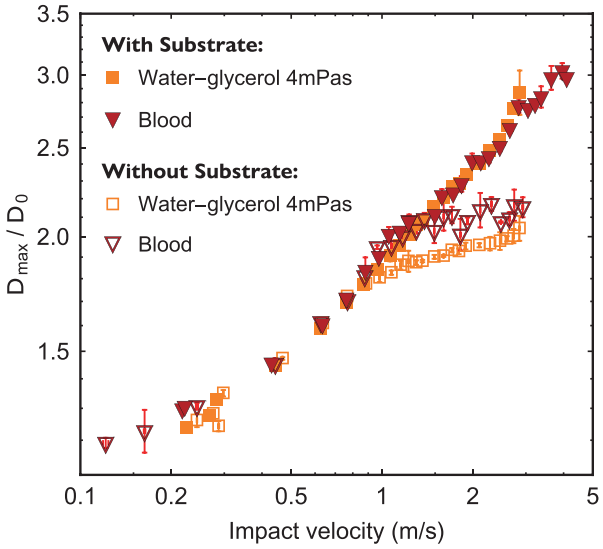

FIG. 7. Measured spreading ratio of a 1:1 water–glycerol mixture ($\eta = 4$ mPa s; orange squares) and blood ($\eta_\infty = 4.8$ mPa s; red triangles) on a 150-μm fabric with and without substrates (filled and open symbols, respectively).

leading to the increased penetration velocity observed in this study. As the viscoelastic behavior in the extensional flow of blood only results in a decrease in the amount of liquid pushing through the fabric, it has no influence on the droplet spreading ratio after the spreading ratio is corrected for the volume loss due to the liquid penetration of the fabric. Thus, we conclude that blood not only spreads like a Newtonian fluid on smooth surfaces,[1] but on fabrics as well.

D. Droplet impact simulations

To determine whether the viscous dissipation inside a spreading droplet is higher when spreading over a fabric, the viscous losses inside the droplet during spreading were determined using an entropic lattice Boltzmann simulation method. With these simulations, the liquid flow velocity v can be calculated inside the droplet during spreading, which subsequently can be used to determine the dissipation function for each simulation time step Φ inside the droplet by calculating the shear rate in each grid node i, j,

$$\Phi = \frac{\mu}{2}\left(\frac{\partial v_i}{\partial x_j} + \frac{\partial v_j}{\partial x_i}\right)^2. \tag{10}$$

The viscous losses inside the droplet during spreading on each simulated surface are shown in Fig. 8. For smooth surfaces, the majority of the viscous dissipation takes place at the interface between the spreading droplet and surface (panels a1–a4). This is expected as the surface generates a significant shear stress inside the liquid during spreading. For the patterned surface (b1–b4) and the fabric attached to the substrate (c1–c4), the viscous dissipation on top of the surface is similar to that of the smooth surface, but there are additional viscous losses inside the pores, caused by the liquid flow filling the pores until they are filled completely. When there is a gap between the fabric and substrate (d1–d4), the liquid is pushed between the fabric and substrate by the solid substrate, leading to viscous losses the moment the liquid pushes itself between the fibers of the fabric and substrate.

For each simulated surface, the total energy lost due to viscous dissipation E_ϕ inside the spreading droplet is determined by summing all viscous losses inside the droplet from the moment of impact up to the moment the droplet reaches maximum spreading. E_ϕ is then normalized with the droplet's total energy E_{tot} [Fig. 8(e)]. On a smooth surface (blue bar), a water droplet loses around 16% of its kinetic energy due to viscous forces during impact. The viscous losses for the patterned surface (purple bar) are significantly higher, indicating that the flow inside the pores indeed leads to an increase in viscous losses, thus confirming that the roughness of the patterned surface has an influence on droplet spreading. Furthermore, the similar viscous dissipation for the patterned surface and fabric that is attached to the surface (no connection between the pores; yellow bar) suggests that the additional surface roughness caused by the weaving of the fabric has no significant influence on the viscous dissipation inside the droplet

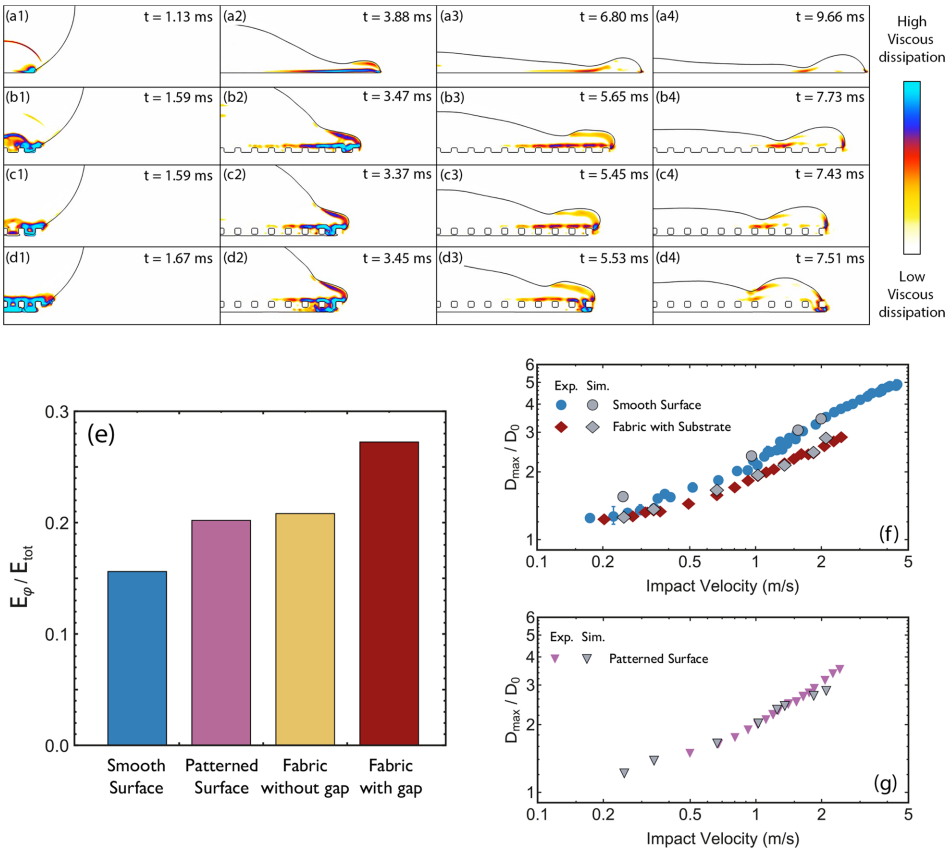

FIG. 8. Three-dimensional simulation results. [(a)–(d)] Cross sections of droplets impacting on a smooth surface (a1–a4), a patterned surface (b1–b4), a fabric on a substrate without a gap (c1–c4), and with a gap (d1–d4) at four subsequent times from the moment of impact to maximum spreading (from left to right). The impact velocity of each droplet is equal to 1.25 m/s. The color scale qualitatively depicts the amount of viscous dissipation inside the droplet, from white (low viscous dissipation) to blue (high viscous dissipation). (e) Ratio of the total dissipated energy with the total energy of the system of a spreading droplet on a smooth surface (blue bar), patterned surface (purple), and fabric without (yellow) and with a gap between the fabric and substrate (red). The total viscous dissipation is determined from the moment of impact up to maximum spreading. (f) Comparison between the measured spreading ratio determined from experiments (colored symbols) and fabric with gap simulations (grey symbols) for the smooth surface (circles) and 150-μm fabric (diamonds). (g) Comparison of the experiments and simulations of droplet spreading on a patterned surface.

and hence on the process of droplet spreading. However, as we only considered a single type of fabric weaving in this study, no definite conclusion can be given. Finally, if the fabric is detached from the substrate, and liquid is allowed to flow in between the fabric and substrate, the viscous dissipation inside the droplet (red bar) significantly increases again compared to the patterned surface.

To determine whether the lower spreading ratios on fabrics are indeed caused by the extra viscous losses inside the droplet, the droplet spreading ratio was determined for the simulated smooth surface, patterned surface, and fabric with a gap. We find that the simulated droplet spreading ratio [Fig. 8(f)] and the experimental measurements [Fig. 8(g)] agree very well. For the smooth surface, the simulated spreading ratio is slightly higher in the low impact velocity regime. Measuring the contact angle with the sessile drop method gave a contact angle hysteresis between 60° and 80°. As mentioned in the Methods, the contact angle hysteresis cannot be accounted for in the simulations for smooth surfaces, and a single contact angle had to be chosen. In this study, a contact angle of 70° was chosen for the smooth surface in the simulations. The difference in droplet spreading ratio between the simulations and experiments at low impact velocity could therefore possibly be attributed to the contact angle hysteresis of the stainless steel surface. Furthermore, roughness effects might also play a role at low impact velocity as the simulated smooth surface was considered to be perfectly smooth and thus less rough than the experimental smooth surface. Low impact velocity spreading is dependent on the wettability of the surface (the advancing contact angle),[4] and thus the higher spreading ratio for the simulation is most likely due to the lower contact angle used in the simulations. The experimental droplet spreading ratio of the patterned surface is described well by the simulations of a smooth patterned surface [Fig. 8(g)] as well. The experimental droplet spreading ratio on fabric with a substrate only agrees well with the simulations for the fabric with a gap [Fig. 8(f)], indicating that the viscous dissipation inside the flow between fabric and substrate is indeed important during droplet impact on fabrics. The simulated droplet spreading ratios for both the patterned surface and fabric with a gap seem to deviate from experiments at the highest simulated impact velocity. However, this deviation is relatively small and is probably caused by errors due to being at a relative high impact velocity. Lattice Boltzmann simulations recover the Navier–Stokes equations plus a higher order error term $O(v^3)$, which is dependent on the impact velocity. Thus, when the impact velocity becomes too high, the error in the simulations significantly reduces the accuracy of the results. Also note that the simulations only consider interactions between the liquid and its vapor, but not the interactions between the liquid and any surrounding gas. It is thus possible, when the vapor pressure changes at the droplet interface during spreading, that the liquid–vapor interactions in the simulations are different from the liquid–air interactions in the experiments at the higher impact velocities. However, no definite conclusion can be given with the results presented here. However, the good agreement between the measured and simulated droplet spreading ratios confirms that the difference in spreading on smooth surfaces and fabrics is indeed due to an increase in viscous losses, which is caused by both the flow into the fabrics pores and the flow in between the fabric and substrate.

The simulations might also help understand why the droplet spreading ratio on the patterned surface becomes comparable to the droplet spreading ratio on smooth surfaces at high impact velocities [Fig. 6(b)]. It is possible that when the droplet spreads over the patterned surface fast enough, the pores are not filled up with liquid as is observed in the simulations [Fig. 8(b1)–8(b4)], but air pockets are trapped inside. In this case, the droplet then "skates" over these air pockets and the extra viscous losses associated with the surface roughness are reduced. At high impact velocities, the viscous dissipation inside a droplet spreading over the patterned surface thus becomes comparable to the viscous losses found for the droplet spreading on a smooth surface. This would lead to an identical droplet spreading ratio for both surfaces. It is important to note here that if the droplet indeed traps air inside the pores of the surface, it creates a "smooth" surface comprised of the surface material and the entrapped air pockets, leading to a Cassie–Baxter like surface that should make the patterned surface more hydrophobic than the smooth surface. However, as was shown by de Goede *et al.*, the surface wettability only influences droplet spreading at low impact velocities ($v < 1$ m/s). As the droplet spreading ratio only becomes comparable at impact velocities above 2 m/s, the influence of the surface wettability is negligible. We do want to point out however that the entrapment of air inside the pores by the droplet is currently only speculation, as the reduced accuracy at high impact velocities and the absence of liquid–air interactions in the simulations currently do not allow to test the hypothesis.

The increase in viscous dissipation during droplet impact is not only observed for fabrics with substrate, but also for fabrics without substrates underneath. For droplet impact simulations on fabrics without substrate [Fig. 9(a)], the extra viscous dissipation originates from the downward flow of the fluid. The liquid pushes itself through the pores in columns that coalesce, leading to the extra viscous dissipation underneath the fabric. The viscous losses inside a droplet pushing through the fabric without a substrate have a significantly higher viscous dissipation ($E_\varphi/E_{tot} = 0.43$) compared to that of a droplet spreading on a smooth surface ($E_\varphi/E_{tot} = 0.16$). The viscous dissipation for the fabric without substrate is also higher compared to the viscous losses for the fabric with a gap ($E_\varphi/E_{tot} = 0.27$), although this can be partly ascribed to the impact velocity being higher for the droplet impact simulation of the fabric without substrate ($v = 1.4$ m/s) compared to that of the simulations on the fabric with substrate ($v = 1.25$ m/s). The spreading ratios obtained from the simulations are slightly lower than those of the experiments [Fig. 9(b)] but still agree well. These measurements show that the extra viscous losses also occur inside the droplet during spreading over fabrics without a substrate.

IV. CONCLUSION

In this study, we investigated the influence of the fabric penetration by the liquid on droplet spreading on monofilament polyester fabrics with pore size much smaller than the initial diameter of the droplet. Using high-speed imaging, we showed that the droplet spreading ratio is influenced by the penetration of the fabric. By applying a volume correction on the droplet spreading ratio on fabrics without substrate, we show that the difference in spreading between fabrics with and without substrate is caused by fabric penetration in the form of liquid volume loss, in agreement with earlier studies. By comparing experiments with entropic lattice Boltzmann simulations, we show that the lower droplet spreading ratio on fabrics at high impact velocities is due to increased viscous losses inside the droplet, which originates from the roughness of the fabric and the droplet pushing itself through the fabric or in between the fabric and substrate during

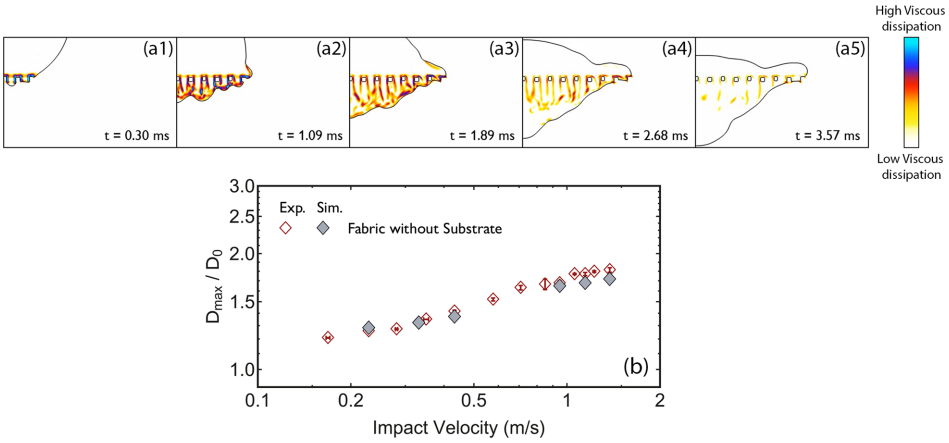

FIG. 9. (a) Viscous dissipation inside a droplet impacting ($v = 1.4$ m/s) on a fabric without substrate shown from the moment of impact ($t = 0$) to maximum spreading. The color scale gives a qualitative depiction of the viscous dissipation from white (low viscous dissipation) to blue (high viscous dissipation). (b) Comparison between experiments (red diamonds) and simulations (black diamonds) of water droplet spreading on fabrics without substrate.

droplet spreading. Finally, although there is a difference in the penetration dynamics for blood, we show that blood can still be approximated as a Newtonian fluid during droplet spreading on fabrics.

Our study shows that droplet spreading is significantly influenced by the fabric geometry for even the most simple of fabrics. As already mentioned in the Introduction, the spreading of normal fluids and blood on textiles is very important, for instance, in the textile industry (stains, rainfasteness, etc.)[33,34] and in forensic research[35–38] where evidence based on bloodstains on clothing and household fabrics is often part of the collected evidence on a crime scene. For applications such as ink-jet printing on textiles, these results could be important: they show that an ink droplet needs to hit the fabric at a higher impact velocity compared to smooth surfaces to cover the same area of fabric. However, our results also show that if the impact velocity becomes too large, the ink can push itself through the fabric and spread out in between the fabric and substrate as well, which can have undesirable effects on the other side of the fabric. Our results also show that, although it is currently not possible to fully determine the total viscous dissipation during droplet spreading on fabrics beforehand, the effect on droplet spreading can be accounted for in the preexisting spreading model on smooth surfaces with an "effective" viscosity that is higher than the actual viscosity of the fluid. The actual value of this effective viscosity is dependent on the fabric geometry and the liquid that spreads over the fabric. Finally, our conclusion that blood spreads similar to a Newtonian fluid on these simple fabrics implies that it is still possible to use the spreading model to find a relation between the size of the bloodstain and the impact velocity of the droplet spreading on a fabric, something that was only currently possible for blood droplets spreading on smooth surfaces.

SUPPLEMENTARY MATERIAL

See the supplementary material for two videos depicting droplet impact on a 150 μm untreated (Movie 1) and plasma treated (Movie 2) fabric mesh.

ACKNOWLEDGMENTS

A.M.M., D.D., and J.C. acknowledge the support by the Swiss National Science Foundation (Project No. 200021_175793). The computational resources were provided by the Swiss National Supercomputing Center (CSCS) under Project No. s823.

DATA AVAILABILITY

The data that support the findings of this study are available from the corresponding author upon reasonable request.

REFERENCES

[1]N. Laan, K. G. de Bruin, D. Bartolo, C. Josserand, and D. Bonn, "Maximum diameter of impacting liquid droplets," Phys. Rev. Appl. **2**, 044018 (2014).
[2]J. B. Lee *et al.*, "Universal rescaling of drop impact on smooth and rough surfaces," J. Fluid Mech. **786**, R4 (2016).
[3]S. Wildeman, C. W. Visser, C. Sun, and D. Lohse, "On the spreading of impacting drops," J. Fluid Mech. **805**, 636–655 (2016).
[4]T. C. de Goede, K. G. de Bruin, N. Shahidzadeh, and D. Bonn, "Predicting the maximum spreading of a liquid drop impacting on a solid surface: Effect of surface tension and entrapped air layer," Phys. Rev. Fluids **4**, 053602 (2019).
[5]G. Riboux and J. M. Gordillo, "Experiments of drops impacting a smooth solid surface: A model of the critical impact speed for drop splashing," Phys. Rev. Lett. **113**, 024507 (2014).
[6]T. C. de Goede, N. Laan, K. G. de Bruin, and D. Bonn, "Effect of wetting on drop splashing of Newtonian fluids and blood," Langmuir **34**, 5163–5168 (2018).
[7]M. A. Quetzeri-Santiago, K. Yokoi, A. A. Castrejón-Pita, and J. R. Castrejón-Pita, "Role of the dynamic contact angle on splashing," Phys. Rev. Lett. **122**, 228001 (2019).
[8]J. M. Kolinski, L. Mahadevan, and S. Rubinstein, "Drops can bounce from perfectly hydrophilic surfaces," Europhys. Lett. **108**, 24001 (2014).
[9]J. de Ruiter, R. Lagraauw, D. van den Ende, and F. Mugele, "Wettability-independent bouncing on flat surfaces mediated by thin air films," Nat. Phys. **11**, 48–53 (2015).
[10]J. de Ruiter, D. van den Ende, and F. Mugele, "Air cushioning in droplet impact. II. Experimental characterization of the air film evolution," Phys. Fluids **27**, 012105 (2015).
[11]L. Xu, W. W. Zhang, and S. R. Nagel, "Drop splashing on a dry smooth surface," Phys. Rev. Lett. **94**, 184505 (2005).
[12]J. San Lee, B. M. Weon, J. H. Je, and K. Fezzaa, "How does an air film evolve into a bubble during drop impact?," Phys. Rev. Lett. **109**, 204501 (2012).
[13]J. M. Kolinski *et al.*, "Skating on a film of air: Drops impacting on a surface," Phys. Rev. Lett. **108**, 074503 (2012).
[14]J. M. Kolinski, L. Mahadevan, and S. M. Rubinstein, "Lift-off instability during the impact of a drop on a solid surface," Phys. Rev. Lett. **112**, 134501 (2014).
[15]J. E. Sprittles, "Air entrainment in dynamic wetting: Knudsen effects and the influence of ambient air pressure," J. Fluid Mech. **769**, 444–481 (2015).
[16]J. E. Sprittles, "Kinetic effects in dynamic wetting," Phys. Rev. Lett. **118**, 114502 (2017).

[17]K. Range and F. Feuillebois, "Influence of surface roughness on liquid drop impact," J. Colloid Interface Sci. **203**, 16–30 (1998).
[18]J. Eggers, M. A. Fontelos, C. Josserand, and S. Zaleski, "Drop dynamics after impact on a solid wall: Theory and simulations," Phys. Fluids **22**, 062101 (2010).
[19]E. W. Collings, A. J. Markworth, J. K. McCoy, and J. H. Saunders, "Splat-quench solidification of freely falling liquid-metal drops by impact on a planar substrate," J. Mater. Sci. **25**, 3677–3682 (1990).
[20]J. Madejski, "Solidification of droplets on a cold surface," Int. J. Heat Mass Transfer **19**, 1009–1013 (1976).
[21]I. V. Roisman, R. Rioboo, and C. Tropea, "Normal impact of a liquid drop on a dry surface: Model for spreading and receding," Proc. R. Soc. London, Ser. A **458**, 1411–1430 (2002).
[22]E. Berthier and D. J. Beebe, "Flow rate analysis of a surface tension driven passive micropump," Lab Chip **7**, 1475–1478 (2007).
[23]J. M. Gordillo, G. Riboux, and E. S. Quintero, "A theory on the spreading of impacting droplets," J. Fluid Mech. **866**, 298–315 (2019).
[24]E. Kissa, "Wetting and wicking," Text. Res. J. **66**, 660–668 (1996).
[25]A. Nyoni and D. Brook, "Wicking mechanisms in yarns-the key to fabric wicking performance," J. Text. Inst. **97**, 119–128 (2006).
[26]S. Benltoufa, F. Fayala, and S. BenNasrallah, "Capillary rise in macro and micro pores of jersey knitting structure," J. Eng. Fibers Fabr. **3**, 47–54 (2008).
[27]P. Brunet, F. Lapierre, F. Zoueshtiagh, V. Thomy, and A. Merlen, "To grate a liquid into tiny droplets by its impact on a hydrophobic microgrid," Appl. Phys. Lett. **95**, 254102 (2009).
[28]S. Ryu, P. Sen, Y. Nam, and C. Lee, "Water penetration through a superhydrophobic mesh during a drop impact," Phys. Rev. Lett. **118**, 014501 (2017).
[29]D. Soto *et al.*, "Droplet fragmentation using a mesh," Phys. Rev. Fluids **3**, 083602 (2018).
[30]A. Kumar, A. Tripathy, Y. Nam, C. Lee, and P. Sen, "Effect of geometrical parameters on rebound of impacting droplets on leaky superhydrophobic meshes," Soft Matter **14**, 1571–1580 (2018).
[31]G. Zhang, M. A. Quetzeri-Santiago, C. A. Stone, L. Botto, and J. R. Castrejón-Pita, "Droplet impact dynamics on textiles," Soft Matter **14**, 8182–8190 (2018).
[32]S. Kooij *et al.*, "Sprays from droplets impacting a mesh," J. Fluid Mech. **871**, 489–509 (2019).
[33]H. Ujiie, *Digital Printing of Textiles* (Woodhead Publishing, 2006).
[34]R. Fangueiro, A. Filgueiras, F. Soutinho, and X. Meidi, "Wicking behavior and drying capability of functional knitted fabrics," Text. Res. J. **80**, 1522–1530 (2010).
[35]E. M. Williams, M. Dodds, M. C. Taylor, J. Li, and S. Michielsen, "Impact dynamics of porcine drip bloodstains on fabrics," Forensic Sci. Int. **262**, 66–72 (2016).
[36]T. C. de Castro, M. C. Taylor, J. A. Kieser, D. J. Carr, and W. Duncan, "Systematic investigation of drip stains on apparel fabrics: The effects of prior-laundering, fibre content and fabric structure on final stain appearance," Forensic Sci. Int. **250**, 98–109 (2015).
[37]X. Li, J. Li, and S. Michielsen, "Effect of yarn structure on wicking and its impact on bloodstain pattern analysis (BPA) on woven cotton fabrics," Forensic Sci. Int. **276**, 41–50 (2017).
[38]F. Wang, V. Gallardo, S. Michielsen, and T. Fang, "Fundamental study of porcine drip bloodstains on fabrics: Blood droplet impact and wicking dynamics," Forensic Sci. Int. **318**, 110614 (2021).
[39]P. Chantelot, M. Coux, C. Clanet, and D. Quéré, "Drop trampoline," Europhys. Lett. **124**, 24003 (2018).
[40]H. Cheng, P. Sun, Y. Tan, Y. Zhang, and X. Wang, "Investigation of single droplet impact on canopy fabric," J. Eng. Fibers Fabr. **14**, 1–13 (2019).
[41]K. Ho and S. Newman, "State of the art electrical discharge machining (EDM)," Int. J. Mach. Tools Manuf. **43**, 1287–1300 (2003).
[42]F. Yilmaz and M. Y. Gundogdu, "A critical review on blood flow in large arteries; relevance to blood rheology, viscosity models, and physiologic conditions," Korea-Aust. Rheol. J. **20**, 197–211 (2008), available at https://www.koreascience.or.kr/article/JAKO200806135610106.page.
[43]A. Mazloomi Moqaddam, S. S. Chikatamarla, and I. V. Karlin, "Entropic lattice Boltzmann method for multiphase flows," Phys. Rev. Lett. **114**, 174502 (2015).
[44]A. Mazloomi Moqaddam, S. S. Chikatamarla, and I. V. Karlin, "Entropic lattice Boltzmann method for multiphase flows: Fluid-solid interfaces," Phys. Rev. E **92**, 023308 (2015).
[45]A. Mazloomi Moqaddam, "Entropic lattice Boltzmann method for two-phase flows," Ph.D. thesis (ETH Zurich, 2016).
[46]A. Mazloomi Moqaddam, S. S. Chikatamarla, and I. V. Karlin, "Simulation of droplets collisions using two-phase entropic lattice Boltzmann method," J. Stat. Phys. **161**, 1420–1433 (2015).
[47]A. Mazloomi Moqaddam, S. S. Chikatamarla, and I. V. Karlin, "Simulation of binary droplet collisions with the entropic lattice Boltzmann method," Phys. Fluids **28**, 022106 (2016).
[48]A. Mazloomi Moqaddam, S. S. Chikatamarla, and I. V. Karlin, "Drops bouncing off macro-textured superhydrophobic surfaces," J. Fluid Mech. **824**, 866–885 (2017).
[49]A. Mazloomi Moqaddam, D. Derome, and J. Carmeliet, "Dynamics of contact line pinning and depinning of droplets evaporating on microribs," Langmuir **34**, 5635–5645 (2018).
[50]M. Slemrod, "Dynamic phase transitions in a van der Waals fluid," J. Differ. Equations **52**, 1–23 (1984).
[51]P. Yuan and L. Schaefer, "Equations of state in a lattice Boltzmann model," Phys. Fluids **18**, 042101 (2006).
[52]P. Chantelot *et al.*, "Water ring-bouncing on repellent singularities," Soft Matter **14**, 2227–2233 (2018).
[53]Y.-L. Hsieh and L. A. Cram, "Enzymatic hydrolysis to improve wetting and absorbency of polyester fabrics," Text. Res. J. **68**, 311–319 (1998).
[54]A. K. Kota, G. Kwon, W. Choi, J. M. Mabry, and A. Tuteja, "Hygro-responsive membranes for effective oil–water separation," Nat. Commun. **3**, 1025 (2012).
[55]K.-C. Park, S. S. Chhatre, S. Srinivasan, R. E. Cohen, and G. H. McKinley, "Optimal design of permeable fiber network structures for fog harvesting," Langmuir **29**, 13269–13277 (2013).
[56]X. Hou, Y. Hu, A. Grinthal, M. Khan, and J. Aizenberg, "Liquid-based gating mechanism with tunable multiphase selectivity and antifouling behaviour," Nature **519**, 70 (2015).
[57]M. Brust *et al.*, "Rheology of human blood plasma: Viscoelastic versus Newtonian behavior," Phys. Rev. Lett. **110**, 078305 (2013).
[58]L. Campo-Deaño, R. P. Dullens, D. G. Aarts, F. T. Pinho, and M. S. Oliveira, "Viscoelasticity of blood and viscoelastic blood analogues for use in polydymethylsiloxane in vitro models of the circulatory system," Biomicrofluidics **7**, 034102 (2013).
[59]S. Kar, A. Kar, K. Chaudhury, T. K. Maiti, and S. Chakraborty, "Formation of blood droplets: Influence of the plasma proteins," ACS Omega **3**, 10967–10973 (2018).